

pubs.acs.org/JACS Article

# Intermolecular Resonance Correlates Electron Pairs Down a Supermolecular Chain: Antiferromagnetism in K-Doped p-Terphenyl

Natalia A. Gadjieva, Péter Szirmai, Olivér Sági, Pere Alemany, Amymarie K. Bartholomew, Ilana Stone, Sergio Conejeros, Daniel W. Paley, Raúl Hernández Sánchez, Brandon Fowler, Samuel R. Peurifoy, Bálint Náfrádi, László Forró, Xavier Roy, Patrick Batail,\* Enric Canadell,\* Michael L. Steigerwald,\* and Colin Nuckolls\*



Cite This: J. Am. Chem. Soc. 2020, 142, 20624–20630



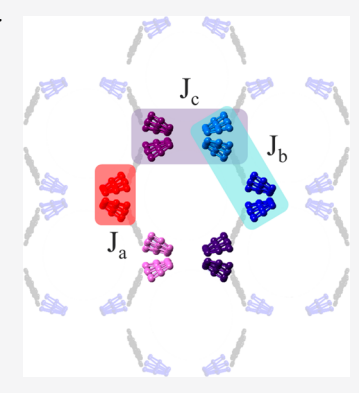
**ACCESS** 

Metrics & More

Article Recommendations

S Supporting Information

**ABSTRACT:** Recent interest in potassium-doped p-terphenyl has been fueled by reports of superconductivity at  $T_c$  values surprisingly high for organic compounds. Despite these interesting properties, studies of the structure—function relationships within these materials have been scarce. Here, we isolate a phase-pure crystal of potassium-doped p-terphenyl:  $[K(222)]_2[p$ -terphenyl $_3$ ]. Emerging antiferromagnetism in the anisotropic structure is studied in depth by magnetometry and electron spin resonance. Combining these experimental results with density functional theory calculations, we describe the antiferromagnetic coupling in this system that occurs in all 3 crystallographic directions. The strongest coupling was found along the ends of the terphenyls, where the additional electron on neighboring p-terphenyls antiferromagnetically couple. This delocalized bonding interaction is reminiscent of the doubly degenerate resonance structure depiction of polyacetylene. These findings hint toward magnetic fluctuation-induced superconductivity in potassium-doped p-terphenyl, which has a close analogy with high  $T_c$  cuprate superconductors. The new approach described here is very versatile as shown by the preparation of two additional salts through systematic changing of the building blocks.



# **■ INTRODUCTION**

Doping of polycyclic aromatic hydrocarbons (PAHs) and fullerenes is known to produce unique emergent properties such as superconductivity, quantum spin liquids, Mott metalinsulator transitions, and antiferromagnetism.<sup>1-7</sup> interest in alkali-doped organics has reemerged after reports of superconductivity with increasing T<sub>c</sub> from K<sub>3</sub>Phenanthrene  $(T_c = 5 \text{ K})^8$  to  $K_{3.3}$ Picene  $(T_c = 18 \text{ K}), ^9 \text{ Cs}_2\text{RbC}_{60}$   $(T_c = 33 \text{ K}), ^{10} \text{ K}_{3.17}$ Dibenzopentacene  $(T_c = 33 \text{ K}), ^{11}$  and the most recent reports of superconductivity of K-doped p-terphenyl with an extremely high  $T_c$  of 123 K. <sup>12</sup> In these systems, there is a dearth of structural data on the molecular packing and the arrangement of the dopant atoms. 1,13,14 Furthermore, reproducibility of superconducting alkali-doped PAHs remains controversial since no repeat experiments on superconductivity at 33 K have been reported. 15 Thus, an understanding of the structure—function relationship in potassium-doped p-terphenyl is of importance to provide design rules for high-temperature superconducting materials from PAHs. The superconducting fraction in the reports on superconductivity in p-terphenyl was found to be low, raising the intriguing possibility that reaction chemistry and crystallography can help understand this important system. Identifying the structure and electronic behavior of ensembles of p-terphenyl radical anions is essential to understanding the superconducting phase and its related properties.

Controlling the reactivity of alkali metals is inherently problematic and contributes to the difficulty of obtaining phase-pure materials. In order to elucidate the fundamental understanding of the alkali metal-doped terphenyl, we developed a new approach based on the ability to controllably modify the building blocks. We report three new phase-pure systems:  $[K(222)]_2[p\text{-terphenyl}_3]$ , [K(222)][methyl-p-terphenyl], and  $[K(18c6)DME]_2[p\text{-terphenyl}_3]$ , where the [2.2.2]Cryptand (222) is a polydentate ligand and 18-crown-6 (18c6) is part of the crown ether family. Both chelating agents selectively encapsulate  $K^+$  ions and thus prevent the alkali metal from forming strong ion— $\pi$  interactions.

Focusing on  $[K(222)]_2[p\text{-terphenyl}_3]$ , crystallography reveals a stoichiometry of three p-terphenyl molecules and two chelated  $K^+$  ions. The crystal contains two different p-terphenyls; the two doped p-terphenyls align as 1D chains around a column of K(222) (Figure 1). In addition to the intermolecular forces that establish the crystalline structure,

Received: May 27, 2020 Published: November 25, 2020





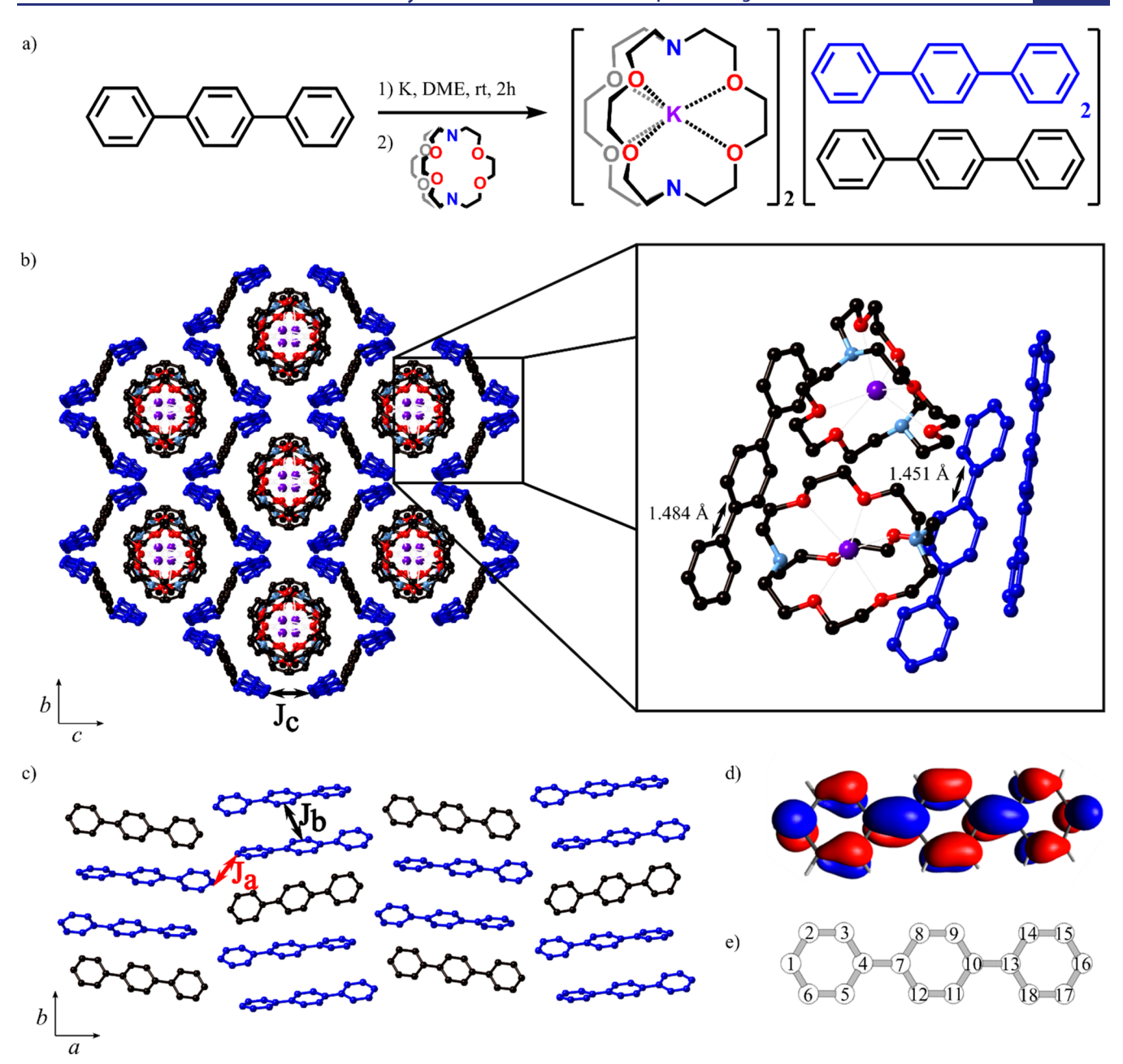


Figure 1. (a) Synthesis of  $[K(222)]_2[p\text{-terphenyl}_3]$ . (b) View of the  $[K(222)]_2[p\text{-terphenyl}_3]$  structure along the a axis with visible channels of (222) chelated to the  $K^+$  ion, surrounded by p-terphenyl molecules. (Inset) Zoom-in on the unit cell, with two unique p-terphenyl, containing a neutral molecule (in black) and doped ones (in blue). Magnetic exchange coupling  $J_c$  between doped p-terphenyl is depicted. (c) View of  $[K(222)]_2[p\text{-terphenyl}_3]$  along the c axis (K(222) removed from the image). Structure shows p-terphenyl radical anions in close proximity along the a axis. Couplings  $J_a$  and  $J_b$  are depicted. (d) Lowest unoccupied molecular orbital (LUMO) of neutral p-terphenyl, showing bonding interactions between phenyl rings and along the long axis of the molecule. (e) Carbon assignment of p-terphenyl.

there are weaker interactions all along the 1D chains; these interactions are best interpreted as weak covalent bonds between adjacent doped terphenyls. Magnetic resonance reveals that the system is antiferromagnetically (AFM) coupled, and DFT calculations show that the coupling is the largest along the p-terphenyl chain.

The appearance of the AFM state in  $[K(222)]_2[p-terpheny]_3$  should be highlighted since a proximity to superconductivity has been made in various systems, including cuprates, Bechgaard salts, and fullerides. Among the latter,  $Cs_3C_{60}$  was found to undergo a transition from an AFM

insulating state to a superconducting state at 38 K under pressure.

Since an attractive interaction between electrons is a requirement to form Cooper pairs, the effective electron—electron interaction emerging in superconductors must overcome the Coulomb repulsion. Although organic superconductors are generally classified as BCS type (Bardeen—Cooper—Schrieffer), the nodal s- or d-wave pairing symmetry for the superconducting gap (if any) is largely an open question for PAHs due to, among other things, the lack of structural data.

### ■ RESULTS AND DISCUSSION

Superconducting materials from doped organics are typically formed by doping a powder, solid-state crystal, or polycrystalline film in the solid state through sublimation of the material.<sup>23-25</sup> However, this method leads to competition between intercalation and decomposition as shown for other PAHs.<sup>26</sup> We find that heating p-terphenyl with potassium metal under vacuum at 120-170 °C for 24-48 h results in a rearrangement and redistribution of the three aromatic rings that make up *p*-terphenyl (see the Supporting Information). To avoid this issue, we dope p-terphenyl with K using a solution-based approach, which was recently employed by Rosseinsky et al. for the alkali doping of phenanthrene. <sup>14</sup> The key is to use a chelating agent, in this case (222), to bind the K<sup>+</sup> ion (Figure 1a). Figure 1b and 1c displays the structure of  $[K(222)]_2[p\text{-terphenyl}_3]$ , as determined by single-crystal X-ray diffraction (SCXRD). Inspecting the unit cell, we see that the structure contains two unique p-terphenyls: one shown in black, and the other two (equivalent) shown in blue. On the basis of the structural parameters of the two types of pterphenyl, we conclude that the blue molecules are anionic while the black ones are neutral. The average interphenyl bond length for the blue p-terphenyl is substantially shorter with values of 1.451 Å (Figure 1e: 4-7 and 10-13), compared to the average 1.484 Å for the black molecule. These distances are consistent with the semiquinoidal structure of the reduced pterphenyl. 19 The other C-C bond lengths lead to the same conclusion, although, as expected, the variations are smaller: the average C-C bonds parallel to the long axis (Figure 1e: 2-3, 5-6, 8-9, 11-12, 14-15, and 17-18) are shorter (1.379 vs 1.386 Å), whereas the average value of the other C-C bonds is larger (1.409 vs 1.396 Å) for the blue p-terphenyls. These observations are consistent with population of the LUMO (Figure 1d) in the blue p-terphenyls, while the black pterphenyls remain thus formally neutral.

The anion of *p*-terphenyl is well known. Gas-phase spectroscopy has shown *p*-terphenyl to have an electron affinity (EA) of 0.4 eV. While this implies that *p*-terphenyl can hold some charge, it does call into question the kinetic stability of the anionic *p*-terphenyl. However, in the solid the anions are stabilized by the electrostatic field of the cations. The simple interpretation that there are two *p*-terphenyl radical anions and one neutral *p*-terphenyl is in fact an oversimplification. Our magnetic and theoretical studies described below show that the system is much more complex due to the low electron affinity of *p*-terphenyl.

We investigated the magnetic properties of  $[K(222)]_2[p-terpheny]_3]$  using magnetic susceptibility and electron spin resonance (ESR) measurements. Figure 2a displays the magnetic susceptibility (measured by SQUID magnetometry). The magnetic susceptibility increases with decreasing temperature, reaching a maximum near 25 K and a subsequent upturn below 10 K. Above 70 K, the susceptibility follows the Curie–Weiss law,  $\chi(T) = \frac{C}{T-\Theta_{CW}}$ , where C is the Curie constant and  $\theta_{CW}$  is the Weiss constant, which gives an estimate of the local magnetic interactions. A fit to the high-temperature data yields  $\theta_{CW} = -60$  K, indicating antiferromagnetic interactions. The effective magnetic moment is calculated to be  $\sim 0.4~\mu_{B}$  per terphenyl at room temperature (see the Supporting Information). As presented below, the Néel temperature was found to be  $T_N = 13$  K from ESR data. The upturn below 10 K may reveal a minute contribution (<2%) of paramagnetic impurities

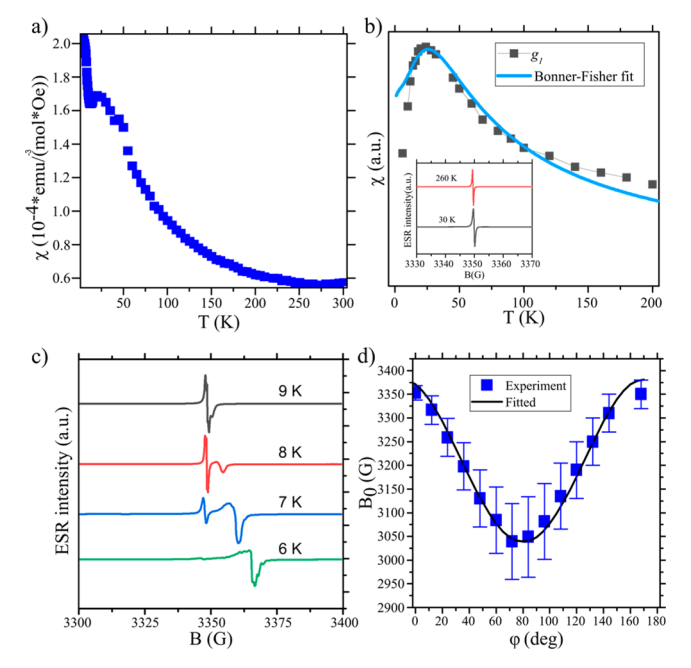


Figure 2. (a) Magnetic susceptibility (FC) measured by SQUID magnetometry at 1 T. Observed feature at 50 K in our SQUID data stems from impurity. (b) Spin susceptibility of [K(222)],[pterphenyl<sub>3</sub>] measured by ESR with  $g_1$  as the dimensionless magnetic moment. Solid line is a fit to the Bonner-Fisher model of spin-1/2 chains. (Inset) Individual ESR spectra of a [K(222)], [p-terphenyl<sub>3</sub>] single crystal. (c) Temperature evolution of the ESR spectra in the AFM state in the Bllb direction at 9.4 GHz. Vanishing ESR signal around B = 3350 G (g = 2) originates from the paramagnetic state. Broad line emerging at higher fields is an AFMR mode stemming from the ordered state. Shift of the AFMR mode (compared to the g =2 paramagnetic signal) decreases with temperature. (d) Angle dependence of the AFMR mode at 9.4 GHz with the magnetic field rotated in the b-c plane at 5 K. Solid line is a fit to an easyintermediate rotation of an AFMR mode with  $\Omega_{-}$  = 3 GHz (and  $\Omega_{+}$  > 50 GHz). Error bars of the points indicate the line width of the AFMR signals.

(see Supporting Information Figure S6). The maximum at 25 K, slightly below the Curie–Weiss temperature, is characteristic of strongly antiferromagnetically (AFM) coupled, low-dimensional systems (Figure 2a).<sup>27</sup>

ESR measurements on a single crystal of  $[K(222)]_2[p-terphenyl_3]$  exhibit a single narrow ( $\sim$ 0.08 mT broad) Lorentzian ESR line above 20 K (see Figure 2b, inset). This narrow ESR signal is typical of exchange-narrowed low-dimensional organic systems.

Temperature-dependent ESR measurements were performed on a single crystal of  $[K(222)]_2[p\text{-terphenyl_3}]$  to track the spin susceptibility of the spin component (Figure 2b). It shows a broad maximum around 25 K, in good agreement with the SQUID magnetic susceptibility data. Below 20 K, we observe an abrupt drop of the paramagnetic ESR signal intensity (Figure 2b). Along with the drop of the susceptibility, the ESR signal in the inset shifts to lower fields (by 0.1-0.2 mT) and broadens slightly. We attribute this to a paramagnetic—antiferromagnetic phase transition. These changes reveal strong antiferromagnetic fluctuations in our system. Interestingly, these emerge only a few Kelvin above the magnetic order, similarly to previously studied antiferromagnets in other low-dimensional organic systems. Specifically, the temperature dependence of the susceptibility resembles that of

quasi-one-dimensional spin chain systems and points to the presence of weak spin anisotropy. This temperature dependence of the susceptibility is described by the Bonner-Fisher model of one-dimensional spin-1/2 chains to fit the ESR spinsusceptibility data above 20 K, shown in blue in Figure 2b.<sup>31</sup> This analysis yields an estimate of dominant, intrachain coupling of 40 K (defined as the coupling corrected by  $k_{\rm B}$ , the Boltzmann constant); we define this coupling as simply  $I_x(x = a, b, or c)$  in the remainder of the text. As shown in Figure 2c, the paramagnetic ESR signal gradually vanishes with temperature below 15 K. At the same time, a new, broad ESR line emerges. This new low-temperature signal is substantially shifted to higher field compared to the paramagnetic ESR signal. Below the antiferromagnetic transition temperature, the spins contributing to the paramagnetic signal adds into the antiferromagnetic phase and give signals at a different field. This new signal is assigned to an antiferromagnetic resonance (AFMR) mode of  $[K(222)]_2[p$ -terphenyl<sub>3</sub>], which is a unique signature—only observed in pure systems—and it captures the spin dynamics of the antiferromagnetic phase.<sup>32</sup>

Through angle-dependent measurements one can identify the magnetic easy, intermediate, and hard axes in an antiferromagnet. The angle and field dependence of the AFMR modes were fitted using a simulation based on the classical mean-field model of Nagamiya and Yosida.<sup>33</sup> The simulation takes the ESR experimental frequency and the resonant field positions as input, and it calculates the deviation of the experimental and theoretical resonant field positions as a function of the easy–intermediate anisotropy energy  $(K_1)$ . The resulting fit is presented in Figure 2d. This yields  $\Omega_{-} = 3$  GHz, which is the measure of the anisotropy in frequency. Figure 2d depicts the angle dependence of the AFMR mode at 9.4 GHz for magnetic field orientations in the b-c plane at 5 K. We conclude that the closely sinusoidal angle dependence stems from an easy-intermediate rotation in the plane. Otherwise, the resonant field position would exhibit a divergent behavior. These AFMR modes combined with our high-frequency ESR studies (see Supporting Information) unambiguously show that the AFM state exhibits triaxial anisotropy in  $[K(222)]_2[p$ terphenyl<sub>3</sub>], meaning that all three axes are magnetically different. In our model, we assign the crystallographic a direction to the hard axis, c to the intermediate axis, and b to the easy axis.

Spin-polarized DFT calculations (see details in the SI) were carried out for different ferromagnetic (FM) and AFM spin configurations of the full lattice. The full AFM configuration (Figure S1) was found to be the most stable spin configuration. The calculations reveal that the negative charge is confined into the subset of blue p-terphenyls. The results of these calculations were indistinguishable from those based only on the blue p-terphenyls sublattice and a background uniform charge, which we used to explore the possible role of disorder (see Supporting Information). The strongest coupling  $(J_a)$  was calculated to be +96 K (where the positive sign refers to AFM interactions) and is along the 1D p-terphenyl chains. This value is in fair agreement with the value of +40 K obtained, as discussed above, from a fit of the experimental data to a simple quasi-one-dimensional spin chain model. The different zigzag chains along a are coupled through interaction  $J_b$  leading to a two-dimensional (ab) network of  $J_a$  and  $J_b$  magnetic interactions, and these planes can couple through  $J_c$  (Figure 1b). The calculated values for  $I_b$  and  $I_c$  are +12 and +36 K, respectively. Consequently, even if, as usual with PerdewBurke—Ernzerhof (PBE)-type calculations, the magnetic interactions are somewhat larger than the experimental ones (see also Figure S2), this study suggests relatively strong AFM interactions along a, weaker AFM interactions along c, and very weak AFM interactions along b, in reasonable agreement with the hard, easy, and intermediate axes assigned with ESR measurements.

The shortest C···C distance associated with interactions  $J_c$  is 4.4 Å (compared to 4.1–4.2 Å for  $J_b$ ), yet  $J_c$  has a larger coupling than  $J_b$ . This initially surprising result can be explained through the LUMO···LUMO interactions (Figure 3a). The C  $2p_z$  orbitals in  $J_c$  are pointed angularly toward each

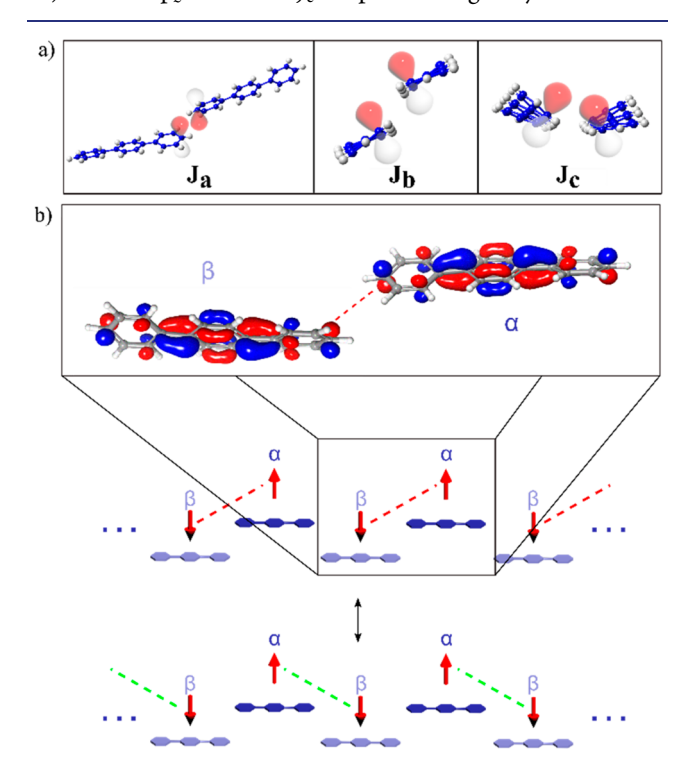


Figure 3. (a) Schematic representation of the three different interactions  $J_{\rm a}>J_{\rm c}>J_{\rm b}$ . Shown are the orbitals providing mostly  $\sigma$ -type orbital overlap in  $J_{\rm a}$ , parallel in  $J_{\rm b}$  and angular toward each other in  $J_{\rm c}$ . Orbitals pictured are simplified representations of the actual orbital shown in Figure 1d. (b) Schematic representation of  $J_{\rm a}$  with two possible resonance structures:  $\alpha-\beta$  electrons interacting on either side of a molecule through red or green coupling. Delocalization of the coupling resembles conjugated systems such as polyacetylene or benzene but rather on a molecular scale introducing intermolecular resonance. (Inset) Red  $\alpha-\beta$  coupling.

other, creating more  $\sigma$  character than in the parallel configured  $J_b$ , consequently creating a better overlap in  $J_c$  than in the parallel configured  $J_b$ . Since the J coupling constants are roughly proportional to the square of the overlaps,  $J_c$  should be stronger than  $J_b$ . An estimation of the LUMO···LUMO overlap integrals associated with the three magnetic coupling interactions leads to a ratio  $(S_a)^2/(S_b)^2/(S_c)^2$  of 5.3/1.0/1.6, in qualitative agreement with the ratio of DFT magnetic coupling constants  $J_a/J_b/J_c$ , 8/1/3. Thus, the conjugated chains of p-terphenyls are mainly coupled through  $J_c$  with a small coupling along  $J_b$ .

From a structure–property perspective,  $[K(222)]_2[p-terphenyl_3]$  exhibits remarkable features with the occurrence of both charged and neutral p-terphenyls as well as chains of p-terphenyl radical anions that couple antiferromagnetically. As

shown by DFT calculations, the two p-terphenyl anions of a ([K(222)]-p-terphenyl), dimeric unit will tend to couple along the a direction. This leads to a  $[trans-(p-terphenyl)_2]^{2-}$  dimer through a somewhat loose C1-C16 bond, i.e., the two "anionic" electrons—one on each terphenyl anion—interact and are low-spin coupled. In such unit, every p-terphenyl anion faces a [K(222)] fragment. Apparently these isolated ([K(222)]-p-terphenyl), dimers are not able to fill space in a compact manner and thus construct a periodic, organic solid having such a high density of localized charge. In order to reach a 1:1 ratio of [K(222)] and p-terphenylanions, the system utilizes an electronically "innocent" unit as structurally and chemically compatible filler. The neutral p-terphenyl fits these requirements. Because of their shape, these neutral molecules are easily adaptable. Moreover, these neutral pterphenyls do not have extra charges that can disturb the packing, and they also have many outer C-H bonds which can make weak hydrogen-bonding interactions that hold the solid together. Under such conditions, the p-terphenyl anions find their way to extend into weakly coupled chains. The extra, "anionic", electrons form weak bonds between adjacent anions, but rather than each p-terphenyl anion forming just a single bond to one of its neighbors, each forms a bond to both of its neighbors along the chain. This seemingly impossible hypervalent situation is the result of valence-bond resonance (as is seen in benzene at the molecular scale and polyacetylene at the extended scale) in which two or more related but distinct bonding patterns constructively interfere (see Figure 3b). It should be emphasized that the resonance structure in our system is intermolecular rather than intramolecular. Furthermore, note that these antiferromagnetically coupled chains can even gain some additional weak stabilization by antiferromagnetically coupling along the interchain directions. This stabilization is the subtle mechanism behind the structure and magnetic properties of  $[K(222)]_2[p\text{-terphenyl}_3]$ .

This approach is versatile; with simple changes in the building blocks we can control the crystal packing and the emergent properties. The power of this approach is that we can change the chelating group for the alkali metal, the PAH, and the alkali metal itself. For example, we produced two other new structures by varying the reaction partners. Changing the chelating group from (222) to (18c6) while keeping the terphenyl constant results in  $[K(18c6)DME]_2[p$ -terphenyl<sub>3</sub>]. This structure has channels of [K(18c6)DME] surrounded by p-terphenyls (Figure 4a). Alternatively, with a slight modification of the PAH we can tune the LUMO of the terphenyl by adding a methyl group on the p-terphenyl, which results in [K(222)][methyl-p-terphenyl] (Figure 4b). The remarkable finding is that the antiferromagnetic ordering persists in each of these chemical cousins (Supporting Information Figures S7 and S8). With these multiple tuning knobs to control the structure, we can now begin developing the rules of correspondence between chemical constituency and physical properties. Such a set of rules will motivate and direct the design of new molecular components. It is not unlikely that these molecules will be much more complex, and their syntheses will be demanding; a roadmap showing the path from intricate molecular components to useful physical properties will inspire these challenging syntheses.

# CONCLUSION

We synthesized and characterized the magnetism of single crystals from phase-pure molecular solids consisting of p-

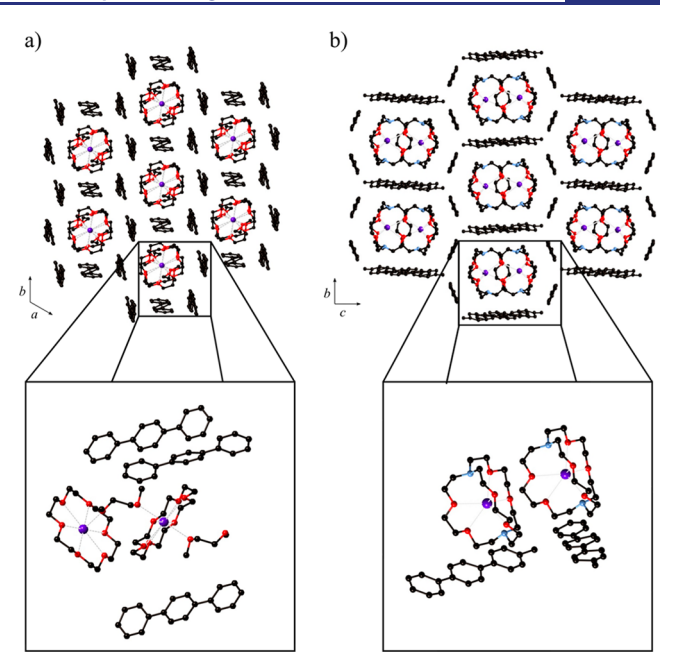


Figure 4. (a) Crystal structure of  $[K(18c6)DME]_2[p\text{-terphenyl}_3]$ . Shown are columns of [K(18c6)DME] surrounded by  $p\text{-terphenyl}_3$ . Zoom-in shows the unit cell with 2 encapsulated  $K^+$  and 3 terphenyls. (b) Crystal structure of [K(222)][p-terphenyl]. Crystal packing shows the same theme of [K(222)] surrounded by methyl-p-terphenyl.

terphenyl, K, and chelating agents. The novelty of the findings is primarily in the ability to control the quality of the structure and its components; this is a significant breakthrough because of the dearth of single crystals of doped PAHs. This result introduces a new generic system amenable to numerous variations of chelated dopants, altogether tuning the stoichiometry and electronic properties, through straightforward synthetic methods. Employment of the (222) cryptand and (18c6) facilitates control over the crystallization process and gives crystalline phases with well-defined stoichiometries; the benefit is invaluable to structural analysis.

We find that in  $[K(222)]_2[p$ -terphenyl<sub>3</sub>] neutral p-terphenyl molecules are interspersed between uniform chains of pterphenyl radical anions, each bearing a 1/2 spin. An AFM phase sets in at 13 K. The observed AFMR (present only in pure systems) provides a clear-cut signature of the threedimensional magnetic order and allows exact determination of the exchange anisotropies. The dominant intrachain antiferromagnetic exchange interaction of 40 K occurs between neighboring p-terphenyls in the chains that run along the a direction. This antiferromagnetic insulator may host high T<sub>c</sub> superconductivity as in the case of hole-doped cuprates. It implies that the high  $T_c$  reported for a polycrystalline K-doped p-terphenyl might be a such minority phase. 34,35 It would be extremely interesting for our high-quality single crystal to explore the phase diagram for both electron and hole doping with the goal of observing superconductivity in a field effect transistor configuration.

# ASSOCIATED CONTENT

# Supporting Information

The Supporting Information is available free of charge at https://pubs.acs.org/doi/10.1021/jacs.0c05606.

Experimental details, ESR explanation, DFT calculations, ESR, SQUID, crystallographic data (PDF) (CIF)

#### AUTHOR INFORMATION

#### Corresponding Authors

Patrick Batail — MOLTECH-Anjou, UMR 6200, CNRS, Universite d'Angers, 49045 Angers, France; Department of Chemistry, Columbia University, New York, New York 10027, United States; orcid.org/0000-0001-7125-5009; Email: patrick.batail@univ-angers.fr

Enric Canadell — Institut de Ciència de Materials de Barcelona (ICMAB-CSIC), Bellaterra 08193, Spain; orcid.org/0000-0002-4663-5226; Email: canadell@icmab.es

Michael L. Steigerwald – Department of Chemistry, Columbia University, New York, New York 10027, United States; Email: mls2064@columbia.edu

Colin Nuckolls — Department of Chemistry, Columbia University, New York, New York 10027, United States; orcid.org/0000-0002-0384-5493; Email: cn37@columbia.edu

# **Authors**

Natalia A. Gadjieva – Department of Chemistry, Columbia University, New York, New York 10027, United States

Péter Szirmai – Laboratory of Physics of Complex Matter, Ecole Polytechnique Fédérale de Lausanne, Lausanne 1015, Switzerland; © orcid.org/0000-0002-2841-5692

Olivér Sági – Laboratory of Physics of Complex Matter, Ecole Polytechnique Fédérale de Lausanne, Lausanne 1015, Switzerland

Pere Alemany – Departament de Ciència de Materials i Química Física and Institut de Química Teòrica i Computacional (IQTCUB), Universitat de Barcelona, Barcelona 08028, Spain; o orcid.org/0000-0002-3139-6189

Amymarie K. Bartholomew – Department of Chemistry, Columbia University, New York, New York 10027, United States

Ilana Stone – Department of Chemistry, Columbia University, New York, New York 10027, United States

Sergio Conejeros — Departamento de Química, Universidad Católica del Norte, Antofagasta 124000, Chile

Daniel W. Paley – Department of Chemistry, Columbia University, New York, New York 10027, United States

Raul Hernandez Sanchez – Department of Chemistry, University of Pittsburgh, Pittsburgh, Pennsylvania 15260, United States; orcid.org/0000-0001-6013-2708

Brandon Fowler – Department of Chemistry, Columbia University, New York, New York 10027, United States

Samuel R. Peurifoy — Department of Chemistry, Columbia University, New York, New York 10027, United States; orcid.org/0000-0003-3875-3035

Bálint Náfradi – Laboratory of Physics of Complex Matter, Ecole Polytechnique Fédérale de Lausanne, Lausanne 1015, Switzerland; orcid.org/0000-0001-9543-2970

László Forró – Laboratory of Complex Matter Physics, Ecole Polytechnique Fédérale de Lausanne, Lausanne 1015, Switzerland

Xavier Roy − Department of Chemistry, Columbia University, New York, New York 10027, United States; ocid.org/ 0000-0002-8850-0725 Complete contact information is available at: https://pubs.acs.org/10.1021/jacs.0c05606

#### **Author Contributions**

The manuscript was written through contributions of all authors. All authors have given approval to the final version of the manuscript.

#### Notes

The authors declare no competing financial interest.

# ACKNOWLEDGMENTS

C.N. thanks Sheldon and Dorothea Buckler for their generous support. Support for this research was provided by the Center for Precision Assembly of Superstratic and Superatomic Solids, an NSF MRSEC (award numbers DMR-1420634 and DMR-2011738), and the Air Force Office of Scientific Research (award number FA9550-18-1-0020). R.H.S. acknowledges support from the Columbia Nano Initiative Postdoctoral Fellowship. X.R. acknowledges support from the NSF CAREER award (NSF DMR-1751949). A.K.B. is supported by the Arnold O. Beckman Fellowship in Chemical Sciences. I.S. is supported by the National Science Foundation under award number CHE-1807654. Single-crystal X-ray diffraction was performed at the Shared Materials Characterization Laboratory at Columbia University, maintained using funding from Columbia University for which we are grateful. Work in Lausanne was supported by the Swiss National Science Foundation. Work in Spain was supported by MICIU (Spain) through Grants PGC2018-096955-B-C44 and PGC2018-093863-B-C22 and Generalitat de Catalunya (2017SGR1506 and 2017SGR1289). E.C. acknowledges support from the Spanish MINECO through the Severo Ochoa Centers of Excellence Program (SEV-2015-0496) and P.A. from the Maria de Maeztu Units of Excellence Program (MDM-2017-0767). S.C. was supported by FONDECYT (Chile) through project 11107163.

# REFERENCES

- (1) Romero, F. D.; Pitcher, M. J.; Hiley, C. I.; Whitehead, G. F. S.; Kar, S.; Ganin, A. Y.; Antypov, D.; Collins, C.; Dyer, M. S.; Klupp, G.; Colman, R. H.; Prassides, K.; Rosseinsky, M. J. Redox-Controlled Potassium Intercalation into Two Polyaromatic Hydrocarbon Solids. *Nat. Chem.* **2017**, *9* (7), 644–652.
- (2) Hebard, A. F.; Rosseinsky, M. J.; Haddon, R. C.; Murphy, D. W.; Glarum, S. H.; Palstra, T. T. M.; Ramirez, A. P.; Kortan, A. R. Superconductivity at 18 K in Potassium-Doped C60. *Nature* **1991**, 350 (6319), 600–601.
- (3) Ganin, A. Y.; Takabayashi, Y.; Khimyak, Y. Z.; Margadonna, S.; Tamai, A.; Rosseinsky, M. J.; Prassides, K. Bulk Superconductivity at 38 K in a Molecular System. *Nat. Mater.* **2008**, *7* (5), 367–371.
- (4) Saito, G.; Yoshida, Y. Organic Superconductors. *Chem. Rec.* **2011**, *11* (3), 124–145.
- (5) Ganin, A. Y.; Takabayashi, Y.; Jeglič, P.; Arčon, D.; Potočnik, A.; Baker, P. J.; Ohishi, Y.; McDonald, M. T.; Tzirakis, M. D.; McLennan, A.; Darling, G. R.; Takata, M.; Rosseinsky, M. J.; Prassides, K. Polymorphism Control of Superconductivity and Magnetism in Cs3 C60 Close to the Mott Transition. *Nature* **2010**, *466* (7303), 221–225
- (6) Craciun, M. F.; Giovannetti, G.; Rogge, S.; Brocks, G.; Morpurgo, A. F.; Van Den Brink, J. Evidence for the Formation of a Mott State in Potassium-Intercalated Pentacene. *Phys. Rev. B: Condens. Matter Mater. Phys.* **2009**, 79 (12), 125116.
- (7) Liu, W.; Lin, H.; Kang, R.; Zhu, X.; Zhang, Y.; Zheng, S.; Wen, H. H. Magnetization of Potassium-Doped P-Terphenyl and P-

- Quaterphenyl by High-Pressure Synthesis. Phys. Rev. B: Condens. Matter Mater. Phys. 2017, 96 (22), 224501.
- (8) Wang, X. F.; Liu, R. H.; Gui, Z.; Xie, Y. L.; Yan, Y. J.; Ying, J. J.; Luo, X. G.; Chen, X. H. Superconductivity at 5 K in Alkali-Metal-Doped Phenanthrene. *Nat. Commun.* **2011**, 2, 507.
- (9) Mitsuhashi, R.; Suzuki, Y.; Yamanari, Y.; Mitamura, H.; Kambe, T.; Ikeda, N.; Okamoto, H.; Fujiwara, A.; Yamaji, M.; Kawasaki, N.; Maniwa, Y.; Kubozono, Y. Superconductivity in Alkali-Metal-Doped Picene. *Nature* **2010**, *464*, *76*.
- (10) Tanigaki, K.; Ebbesen, T. W.; Saito, S.; Mizuki, J.; Tsai, J. S.; Kubo, Y.; Kuroshima, S. Superconductivity at 33 K in Cs, Rb, C<sub>60</sub>. *Nature* **1991**, 352, 222–223.
- (11) Xue, M.; Cao, T.; Wang, D.; Wu, Y.; Yang, H.; Dong, X.; He, J.; Li, F.; Chen, G. F. Superconductivity above 30 K in Alkali-Metal-Doped Hydrocarbon. Sci. Rep. 2012, 2, 389.
- (12) Wang, R.-S.; Gao, Y.; Huang, Z.-B.; Chen, X.-J. Superconductivity above 120 K in a Chain Link Molecule. *arXiv* **2017**, 1–19.
- (13) Kosugi, T.; Miyake, T.; Ishibashi, S.; Arita, R.; Aoki, H. First-Principles Electronic Structure of Solid Picene. *J. Phys. Soc. Jpn.* **2009**, 78, 113704.
- (14) Takabayashi, Y.; Menelaou, M.; Tamura, H.; Takemori, N.; Koretsune, T.; Štefančič, A.; Klupp, G.; Buurma, A. J. C.; Nomura, Y.; Arita, R.; Arčon, D.; Rosseinsky, M. J.; Prassides, K. π-Electron S = 1/2 Quantum Spin-Liquid State in an Ionic Polyaromatic Hydrocarbon. *Nat. Chem.* **2017**, *9* (7), 635–643.
- (15) Heguri, S.; Kobayashi, M.; Tanigaki, K. Questioning the Existence of Superconducting Potassium Doped Phases for Aromatic Hydrocarbons. *Phys. Rev. B: Condens. Matter Mater. Phys.* **2015**, 92 (1), 014502.
- (16) Rosseinsky, M. J.; Murphy, D. W.; Fleming, R. M.; Tycko, R.; Ramirez, A. P.; Dabbagh, G.; Barrett, S. E. Structural and Electronic Properties of Sodium-Intercalated C60. *Nature* **1992**, *356* (6368), 416–418.
- (17) Park, K. Quantum Antiferromagnetism and High Tc Superconductivity: A Close Connection between the t-J Model and the Projected BCS Hamiltonian. *Phys. Rev. B: Condens. Matter Mater. Phys.* **2005**, 72 (24), 245116.
- (18) Bourbonnais, C.; Sedeki, A. Link between Antiferromagnetism and Superconductivity Probed by Nuclear Spin Relaxation in Organic Conductors. *Phys. Rev. B: Condens. Matter Mater. Phys.* **2009**, *80* (8), 085105.
- (19) Takabayashi, Y.; Ganin, A. Y.; Jeglič, P.; Arčon, D.; Takano, T.; Iwasa, Y.; Ohishi, Y.; Takata, M.; Takeshita, N.; Prassides, K.; Rosseinsky, M. J. The Disorder-Free Non-BCS Superconductor Cs<sub>3</sub>C<sub>60</sub> Emerges from an Antiferromagnetic Insulator Parent State. *Science (Washington, DC, U. S.)* **2009**, 323 (5921), 1585–1590.
- (20) Kawamoto, A.; Miyagawa, K.; Nakazawa, Y.; Kanoda, K. ~3C NMR Study of Layered Organic Superconductors Based on BEDT-TTF Molecules. *Phys. Rev. Lett.* **1995**, *74* (17), 3455–3458.
- (21) Miyagawa, K.; Kanoda, K.; Kawamoto, A. NMR Studies on Two-Dimensional Molecular Conductors and Superconductors: Mott Transition in K-(BEDT-TTF)<sub>2</sub>X. Chem. Rev. 2004, 104, 5635–5654.
- (22) Zantout, K.; Altmeyer, M.; Backes, S.; Valenti, R. Superconductivity in correlated BEDT-TTF molecular conductors: Critical temperatures and gap symmetries. *Phys. Rev. B: Condens. Matter Mater. Phys.* **2018**, 97, 014530.
- (23) Wang, P.; Metzger, R. M.; Bandow, S.; Maruyama, Y. Superconductivity in Langmuir-Blodgett Multilayers of C60 Doped with Potassium. *J. Phys. Chem.* **1993**, *97* (12), 2926–2927.
- (24) Miura, Y. F.; Horikiri, M.; Saito, S. H.; Sugi, M. Evidence for Superconductivity in Langmuir-Blodgett Films of Ditetradecyldimethylammonium-Au(Dmit)2. *Solid State Commun.* **2000**, *113* (11), 603–605.
- (25) Kubozono, Y.; Mitamura, H.; Lee, X.; He, X.; Yamanari, Y.; Takahashi, Y.; Suzuki, Y.; Kaji, Y.; Eguchi, R.; Akaike, K.; Kambe, T.; Okamoto, H.; Fujiwara, A.; Kato, T.; Kosugi, T.; Aoki, H. Metal-Intercalated Aromatic Hydrocarbons: A New Class of Carbon-Based Superconductors. *Phys. Chem. Chem. Phys.* **2011**, *13*, 16476–16493.

- (26) Zhang, J.; Whitehead, G. F. S.; Manning, T. D.; Stewart, D.; Hiley, C. I.; Pitcher, M. J.; Jansat, S.; Prassides, K.; Rosseinsky, M. J. Reactivity of Solid Rubrene with Potassium: Competition between Intercalation and Molecular Decomposition. *J. Am. Chem. Soc.* **2018**, 140 (51), 18162–18172.
- (27) Torrance, J. B.; Tomkiewicz, Y.; Silverman, B. D. Enhancement of the Magnetic Susceptibility of TTF-TCNQ (Tetrathiafulvalene-Tetracyanoquinodimethane) by Coulomb Correlations. *Phys. Rev. B* **1977**, *15* (10), 4738–4749.
- (28) Náfrádi, B.; Olariu, A.; Forró, L.; Mézière, C.; Batail, P.; Jánossy, A. Spin Dynamics in the S=1/2 Antiferromagnetic Chain Compounds  $\delta$ -(EDT-TTF-CONMe<sub>2</sub>)<sub>2</sub> X (X = AsF<sub>6</sub>, Br): A Multi-Frequency Electron Spin Resonance Study. *Phys. Rev. B: Condens. Matter Mater. Phys.* **2010**, 81 (22), 224438.
- (29) Dumm, M.; Loidl, A.; Fravel, B. W.; Starkey, K. P.; Montgomery, L. K.; Dressel, M. Electron Spin Resonance Studies on the Organic Linear-Chain Compounds (TMTCF)<sub>2</sub>X (C = S, Se; X = PF<sub>6</sub>, AsF<sub>6</sub>, ClO<sub>4</sub>, Br). *Phys. Rev. B: Condens. Matter Mater. Phys.* **2000**, *61*, 511.
- (30) Zheng, W.; Singh, R. R. P.; Mckenzie, R. H.; Coldea, R. Temperature Dependence of the Magnetic Susceptibility for Triangular-Lattice Antiferromagnets with Spatially Anisotropic Exchange Constants. *Phys. Rev. B: Condens. Matter Mater. Phys.* **2005**, 71, 134422.
- (31) Bonner, J. C.; Fisher, M. E. Linear Magnetic Chains with Anisotropic Coupling. *Phys. Rev.* **1964**, *135* (3A), A640.
- (32) Coulon, C.; Clérac, R. Electron Spin Resonance: a major probe for molecular conductors. *Chem. Rev.* **2004**, *104*, 5655–5687.
- (33) Nagamiya, T.; Yosida, K.; Kubo, R. Antiferromagnetism. *Adv. Phys.* **1955**, *4* (13), 1–112.
- (34) Slezak, J. A.; Lee, J.; Wang, M.; McElroy, K.; Fujita, K.; Andersen, B. M.; Hirschfeld, P. J.; Eisaki, H.; Uchida, S.; Davis, J. C. Imaging the impact on cuprate superconductivity of varying the interatomic distances within individual crystal unit cells. *Proc. Natl. Acad. Sci. U. S. A.* **2008**, *105* (9), 3203–3208.
- (35) Mori, T. Organic Conductors with Unusual Band Fillings. Chem. Rev. 2004, 104 (11), 4947–4969.